

# Renal and Visceral Artery Configuration During the First Year of Follow-Up After Fenestrated Aortic Aneurysm Repair Using the Anaconda Stent-graft: A Prospective Longitudinal Multicenter Study With ECG-Gated CTA Scans

Journal of Endovascular Therapy  
 1–12

© The Author(s) 2023



Article reuse guidelines:

sagepub.com/journals-permissions

DOI: 10.1177/15266028231209929

www.jevt.org



Jaimy A. Simmering, PhD<sup>1,2</sup> , Maaïke A. Koenrades, PhD<sup>1,2,3</sup> ,  
 Cornelis H. Slump, PhD<sup>4</sup>, Erik Groot Jebbink, PhD<sup>2,5</sup> ,  
 Clark J. Zeebregts, PhD, MD<sup>6</sup>, Michel M.P.J. Reijnen, PhD, MD<sup>2,5</sup>,  
 and Robert H. Geelkerken, PhD, MD<sup>1,2</sup>

## Abstract

**Objective:** The performance of fenestrated endovascular aortic aneurysm repair (FEVAR) may be compromised by complications related to the dynamic vascular environment. The aim of this study was to analyze the behavior of FEVAR bridging stent configurations during the cardiac cycle and during follow-up to improve our understanding on treatment durability.

**Design:** Twenty-one patients presenting with complex abdominal aortic aneurysms (AAAs; 9 juxtarenal/6 pararenal/3 paravisceral/1 thoracoabdominal aortic aneurysm type IV), treated with a fenestrated Anaconda (Terumo Aortic, Inchinnan, Scotland, UK) with Advanta V12 bridging stents (Getinge, Merrimack, NH, USA), were prospectively enrolled in a multicenter observational cohort study and underwent electrocardiogram (ECG)-gated computed tomographic angiography (CTA) preoperatively, at discharge, 7-week, and 12-month follow-ups.

**Methods:** Fenestrated endovascular aortic aneurysm repair stability was assessed considering the following variables: branch angle as the angle between the aorta and the target artery, end-stent angle as the angle between the end of the bridging stent and the native artery downstream from it, curvature and tortuosity index (TI) to describe the bending of the target artery. Body-bridging stent stability was assessed considering bridging stent flare lengths, the distances between the proximal sealing stent-ring and fenestrations and the distance between the fenestration and first apposition in the target artery.

**Results:** Renal branch angles significantly increased after FEVAR toward a perpendicular position (right renal artery from median 60.9°, inter quartile range [IQR]=44.2–84.9° preoperatively to 94.4°, IQR=72.6–99.8°,  $p=0.001$  at 12-month follow-up; left renal artery [LRA], from 63.7°, IQR=55.0–73.0° to 94.3°, IQR=68.2–105.6°,  $p<0.001$ ), while visceral branch angles did not. The mean dynamic curvature only decreased for the LRA from preoperative (3.0, IQR=2.2–3.8  $m^{-1}$ ) to 12-month follow-up (1.9, IQR=1.4–2.6  $m^{-1}$ ,  $p=0.027$ ). The remaining investigated variables did not seem to show any changes over time in this cohort.

**Conclusions:** Fenestrated endovascular aortic aneurysm repair for complex AAAs using the Anaconda fenestrated stent-graft and balloon-expandable Advanta V12 bridging stents demonstrated stable configurations up to 12-month follow-up, except for increasing renal branch angles toward perpendicular orientation to the aorta, yet without apparent clinical consequences in this cohort.

## Clinical Impact

This study provides detailed information on the cardiac-pulsatility-induced (dynamic) and longitudinal geometry deformations of the target arteries and bridging stents after fenestrated endovascular aortic aneurysm repair (FEVAR) up to 12-month follow-up. The configuration demonstrated limited dynamic and longitudinal deformations in terms of branch angle, end-stent angle, curvature, and tortuosity index (TI), except for the increasing renal branch angles that go toward a perpendicular orientation to the aorta. Overall, the results suggest that the investigated FEVAR configurations are stable and durable, though careful consideration of increasing renal branch angles and significant geometry alterations is advised.

## Keywords

fenestrated endovascular aortic aneurysm repair, ECG-gated computed tomography, bridging stent, geometry, dynamic, cardiac-pulsatility-induced

## Introduction

Fenestrated endovascular aortic aneurysm repair (FEVAR) is used to treat complex abdominal aortic aneurysms (AAAs), while maintaining perfusion of the renal-mesenteric arteries using fenestrations in the main stent-graft, combined with bridging stents.<sup>1</sup> Fenestrated endovascular aortic aneurysm repair has reported high technical success rates of 84% to 100%,<sup>2-4</sup> 30-day mortality rates of 0% to 7%,<sup>3-6</sup> and 1-year reintervention-free survival rate of 80% to 96%.<sup>2,6-8</sup> Nevertheless, the performance of these stent-grafts can be compromised by complications requiring reintervention in 16% to 24% of the patients through 3- to 4-year follow-up.<sup>9,10</sup> Follow-up after FEVAR is routinely performed using static computed tomographic angiography (CTA) to detect potential complications, such as migration, kinking, stent fractures, stenosis or occlusion, and endoleaks.<sup>1</sup> However, static imaging techniques do not consider the aortic motion, which is likely to influence FEVAR performance.<sup>11,12</sup> Consequently, the cardiac-pulsatility-induced (dynamic) deformation of the stented target arteries, and the subsequent challenges to FEVAR durability, are currently not fully understood. Besides cardiac induced motion, respiratory motion may also play an important role.<sup>13</sup> However, the present study focused on the cardiac pulsatility induced deformation. Electrical cardiogram (ECG)-gated CTA, also 4D (3D+t) or dynamic CTA, is a technique that takes the patient's cardiac cycle into account, enabling studies on the dynamic deformation of the aorta and its branches, together with implanted devices.<sup>14-18</sup> When performed in a longitudinal fashion with multiple ECG-gated CTAs during follow-up, the longitudinal deformation of stent-grafts can be investigated as well.<sup>14,17,19</sup> The dynamic and longitudinal deformation of the renal and visceral arteries have been investigated sparsely,<sup>16,20-22</sup> and knowledge about the interaction between arteries and stent-graft components remains limited. The aim of this study was to obtain detailed information on the dynamic and longitudinal deformation of the

FEVAR target arteries and bridging stents to improve our understanding about device stability.

## Methods

### Study Design

From February 2017 to December 2020, consecutive asymptomatic complex AAA patients treated with the fenestrated Anaconda stent-graft (Terumo Aortic, Inchinnan, Scotland, UK) in 3 experienced sites were prospectively enrolled in a multicenter observational cohort study ([LSPEAS F-EVAR]; registered at [trialsearch.who.int](http://trialsearch.who.int), identifier NTR6225). Inclusion and exclusion criteria can be found in Table 1. Patient selection for FEVAR occurred according to the European Society for Vascular Surgery (ESVS) guidelines<sup>23</sup> and was a shared decision by patient and treating physician, taking into account the advice resulting from a multidisciplinary team discussion regarding patient frailty, anatomy and technical possibilities, and consultation with the manufacturer. The study protocol included 4 ECG-gated CTA scans at predetermined timepoints: pre-operative, before discharge, and at 7-week and 12-month follow-ups. Patient and aneurysm characteristics were collected according to reporting standards.<sup>24</sup> The study protocol was approved by the ethical committee (NL59794.044.16) and the institutional review boards. Written informed consent was obtained from each subject prior to participation. All patient-related data were processed anonymously and stored electronically in agreement with the Declaration of Helsinki-Ethical principles for medical research involving human subjects.

### Image Acquisition and Processing

Electrocardiogram-gated CTAs were obtained on a Somatom Definition Flash (Siemens Healthineers, Erlangen, Germany) or a Brilliance iCT 256-slice CT scanner (Philips Healthcare, Best, The Netherlands) with scan protocols based on routine

<sup>1</sup>Department of Surgery (Division of Vascular Surgery), Medisch Spectrum Twente, Enschede, the Netherlands

<sup>2</sup>Multi-modality Medical Imaging (M3i) Group, Faculty of Science and Technology, Technical Medical Centre, University of Twente, Enschede, the Netherlands

<sup>3</sup>Medical 3D Lab, Medisch Spectrum Twente, Enschede, the Netherlands

<sup>4</sup>Robotics and Mechatronics (RaM) Group, Faculty of Electrical Engineering, Mathematics and Computer Science, Technical Medical Centre, University of Twente, Enschede, the Netherlands

<sup>5</sup>Department of Surgery, Rijnstate, Arnhem, the Netherlands

<sup>6</sup>Division of Vascular Surgery, Department of Surgery, University Medical Center Groningen, University of Groningen, Groningen, the Netherlands

### Corresponding Author:

Jaimy A. Simmering, Multi-Modality Medical Imaging (M3i) Group, Faculty of Science and Technology, Technical Medical Centre, University of Twente, PO Box 217, 7500 AE Enschede, the Netherlands.

Email: [j.a.simmering@utwente.nl](mailto:j.a.simmering@utwente.nl)

**Table 1.** Inclusion and Exclusion Criteria for the LSPEAS F-EVAR Trial.

Inclusion criteria	Exclusion criteria
Asymptomatic AAA	No informed consent obtained
Age > 65*	eGFR < 30 mL/min
Indication for AAA treatment according to standard practice	Allergy for intra venous contrast fluid
Anatomic suitability for the Fenestrated Anaconda™ stent-graft	
At least, 1 stentable main renal artery and 1 other stentable renal or mesenteric artery	

\*Due to ethical considerations regarding radiation exposure, a minimum age requirement was set for inclusion in this trial.

AAA scan protocols, respecting the “as low as reasonably achievable” (ALARA) principle. Acquisition was during breath hold with the following scan parameters: tube voltage 120 kV; tube current by automated tube modulation; collimation  $2 \times 64 \times 0.6$  mm (Siemens) or  $128 \times 0.6$  (Philips); slice thickness 1 mm; slice increment 0.5 mm; reconstruction matrix  $512 \times 512$  pixels resulting in  $0.5 \times 0.5 \times 1$  mm voxels with reconstruction kernel I36f (Siemens) or iDose (Philips). The pitch factor was set automatically based on the heart rate. Eighty milliliter of intravenous contrast agent administration at 4 mL/s with bolus tracking at the proximal abdominal aorta and image acquisition starting 12 seconds after the signal density peak. Retrospective gating based on the RR-interval was applied to reconstruct 10 equidistant volumes covering the cardiac cycle (0%–90%).

For each CTA, the 10 reconstructed volumes were registered to a single static phase-averaged volume with improved resolution and signal-to-noise ratio using a previously defined registration algorithm.<sup>25–28</sup> This registration also provides deformation fields to translate measurement in the phase-averaged volume back to the original phases and thereby diminishing user dependence in the dynamic analysis. All image processing and analyses were performed by algorithms in Python programming language (version 3.7).

### Dynamic and Longitudinal Target Artery Geometry and Stability

A wide range of variables were calculated from the CTA data to investigate the dynamic and longitudinal changes in geometry and stability of the fenestrated Anaconda. The variables were chosen based on previously established value and the authors’ discretion.<sup>11,18,29–33</sup> The dynamic variables were defined as the largest minus the smallest value during the cardiac cycle.

**Centerline calculation** was performed using an established in-house written algorithm<sup>16,17,34</sup> to obtain center lumen lines (CLLs) used to calculate the geometrical variables branch angle, end-stent angle, curvature, and tortuosity index (TI). The centerlines were created semi-automatically with only the general location of the start and endpoint of the line being obtained manually, although these points were excluded from analyses. A branch CLL ( $CLL_{branch}$ ) runs from the ostium to the first bifurcation of the target artery, based on vessel and stent threshold segmentations (150 and 500 Hounsfield units, respectively); an aorta CLL ( $CLL_{aorta}$ ) is calculated based on the vessel segmentation. The CLLs were obtained in the phase-averaged CTA volume to assess longitudinal variable changes. The CLLs were translated to the different cardiac phases to calculate the dynamic variable changes.

**Branch angle** is the angle between the target artery and the aorta (Figure 1A) and is calculated between the branch vector and the aorta vector.<sup>16</sup> The branch vector is a 10 mm vector along the first 10 mm of the  $CLL_{branch}$  and the aorta vector is a 10 mm vector on the  $CLL_{aorta}$  with its center at the  $CLL_{aorta}$  point closest to  $CLL_{branch}$  start. A 90° branch angle indicates the target artery is perpendicular to the aorta.

**End-stent angle** is the angle between the end of the bridging stent and the native artery downstream from it.<sup>11</sup> Figure 1A shows that the end-stent angle is calculated between 2 vectors along the  $CLL_{branch}$  at the end of the bridging stent: a 10 mm upstream vector, that is, the stent vector, and a downstream vector, that is, the artery vector. The length of the artery vector toward the first bifurcation was limited to 10 mm. For preoperative measurements the end of the bridging stent was defined by projection of the first post-operative stented arc length over the preoperative  $CLL_{branch}$ . In case of temporary post-FEVAR renal impairment, a CTA was made without contrast administration, in which case the end-stent angles could not be calculated. A 0° end-stent angle indicates a straight  $CLL_{branch}$  at the end of the bridging stent.

**Curvature** describes the bending of the CLL and can be interpreted as the inverse of the radius of a locally fitted circle to the CLL (Figure 1B). The curvature was obtained for each  $CLL_{branch}$  point by numerical calculation as elaborated on in previous publications.<sup>17,18</sup> Mean and maximal curvature are the average and maximal value calculated of all  $CLL_{branch}$  points, respectively. The dynamic curvature was calculated for each individual  $CLL_{branch}$  point as the difference between the highest and lowest value for that  $CLL_{branch}$  point after translating the  $CLL_{branch}$  to the individual cardiac phases and calculating curvature for the phase-CLLs. Mean and maximal dynamic curvature change were calculated as the mean and maximal value of the dynamic curvature of all  $CLL_{branch}$  points, respectively. A decrease in curvature indicates straightening of the target artery and smaller dynamic curvature indicates less bending

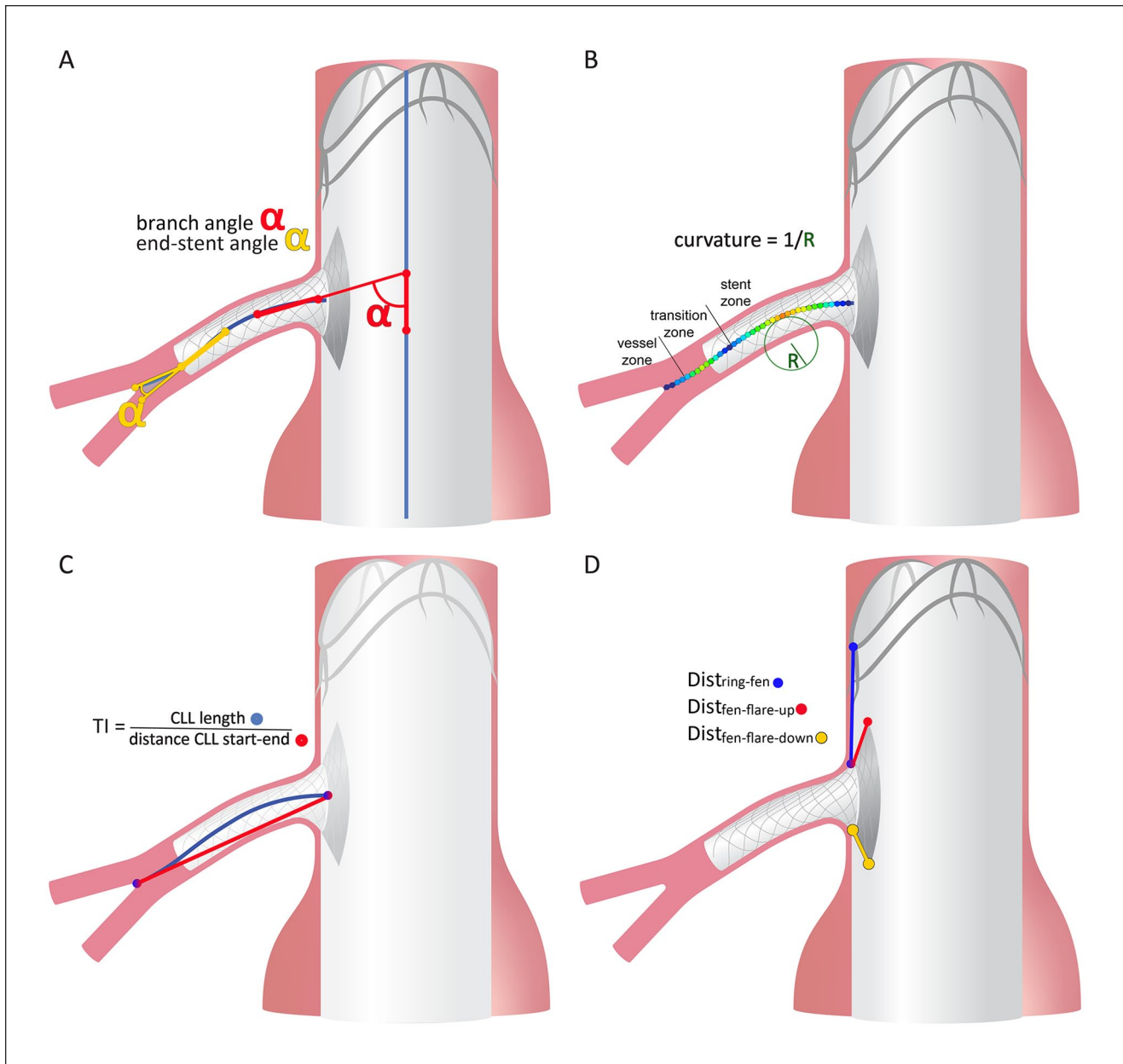


**Figure 1.** Schematic representation of the measurements on the fenestrated Anaconda target arteries and bridging stents. The measurements describe (A) the branch angle (red  $\alpha$ ) as the angle between the aortic center lumen line (CLL<sub>aorta</sub>, blue) vector and the branch CLL vector (CLL<sub>branch</sub>, blue), and the end-stent angle (yellow  $\alpha$ ) as the angle between the CLL<sub>branch</sub> stent vector and vessel vector; (B) the color-coded curvature over the CLL<sub>branch</sub> with a larger (dynamic) curvature presented in red and a small (dynamic) curvature presented in blue. In 2 dimensions, curvature can be described as the inverse of the radius R of the circle following the CLL. The location of the maximal curvature was classified in the stented part of the CLL (stent zone), the downstream vessel part of the CLL (vessel zone) or the 10 mm transition zone covering the last 5 mm of stented CLL and first 5 mm of vessel CLL; (C) the tortuosity index (TI) as the ratio between the length of the CLL<sub>branch</sub> (blue) and the straight distance from start to end point of the CLL<sub>branch</sub> (red); (D) the distances between different elements of the body and bridging stents: the proximal stent-ring peak or valley above the fenestration to the fenestration (Dist<sub>ring-fen</sub>, blue) and flare lengths on the upstream or downstream end of the fenestration (Dist<sub>fen-flare-up</sub>, red and Dist<sub>fen-flare-down</sub>, yellow, respectively).

deformation during the cardiac cycle, that is, stiffening of the target artery. Curvature geometry change is location-dependent, and so that, the location of maximal (dynamic)

curvature was categorized into the stent zone, vessel zone, or transition zone. The transition zone covers the 10 mm around the end of the bridging stent (Figure 1B).

**Tortuosity index** of the target artery is calculated as the ratio between the length of the  $CLL_{branch}$  and the straight distance from start to end of the  $CLL_{branch}$  (Figure 1C).<sup>24</sup> Similar to (mean) curvature, a decrease in TI indicates the target artery becomes less tortuous, that is, straightened, and a decrease in dynamic  $\Delta$  TI indicates less deformation during the cardiac cycle, that is stiffening.

**Body-bridging stent stability** was investigated by evaluation of distances between different elements of the FEVAR body and bridging stents: the distance between fenestration and the peak or valley on the proximal sealing stent-ring above the fenestration ( $Dist_{ring-fen}$ ), the flare lengths as the distance between the fenestration and the flare of the bridging stent in upstream and downstream directions ( $Dist_{fen-flare-up}$  and  $Dist_{fen-flare-down}$ , respectively, Figure 1D), and the fenestration gap, that is, the distance between the fenestration in the main body and the start of the bridging stent apposition in the target artery, as defined by Chait et al.<sup>35</sup> The upstream fenestration border was defined as the center of the 2 upstream fenestration radiopaque markers. Likewise, the downstream fenestration border was defined as the center of the 2 downstream markers. The stent-ring's peaks and valleys, radiopaque markers, and flares were manually selected in a 3D maximal intensity projection (MIP) of the phase-averaged CTA volume. For dynamic distances the selected locations were translated to the individual cardiac phases. The dynamic fenestration gap was not obtained because of the limited signal to noise ratio in the individual phases of the CT scans, hampering proper distinguishing of the aortic wall in endovascular aortic aneurysm repair (EVAR) planning software (Aquarius Intuition, TeraRecon, Inc., Foster City, California, USA) as recommended by Chait et al.<sup>35</sup> Decrease in  $Dist_{ring-fen}$  may indicate migration of the proximal sealing stent-rings and decrease in  $Dist_{fen-flare-up}$  and/or  $Dist_{fen-flare-down}$  may indicate outward migration of the bridging stent. A difference in change in  $Dist_{fen-flare-up}$  and  $Dist_{fen-flare-down}$  may indicate pivoting of the bridging stent. Larger fenestration gaps may be associated with target artery instability after FEVAR.<sup>35</sup>

### Statistical Analysis

The distribution of the data was checked by visual inspection of histograms. All data were found to be normally distributed. Continuous data were presented as median (interquartile range, IQR) and categorical data as n (%). Longitudinal change in the variables was analyzed with linear mixed-model repeated measures analysis with a post-hoc Bonferroni correction for multiple measurements, presented as change (standard error [SE], 95% confidence interval [CI], and p value). Change in location of maximal curvature was assessed with Pearson's McNemar-Bowker test. Paired samples *t*-tests were used to compare the upstream and downstream flare lengths, presented as mean

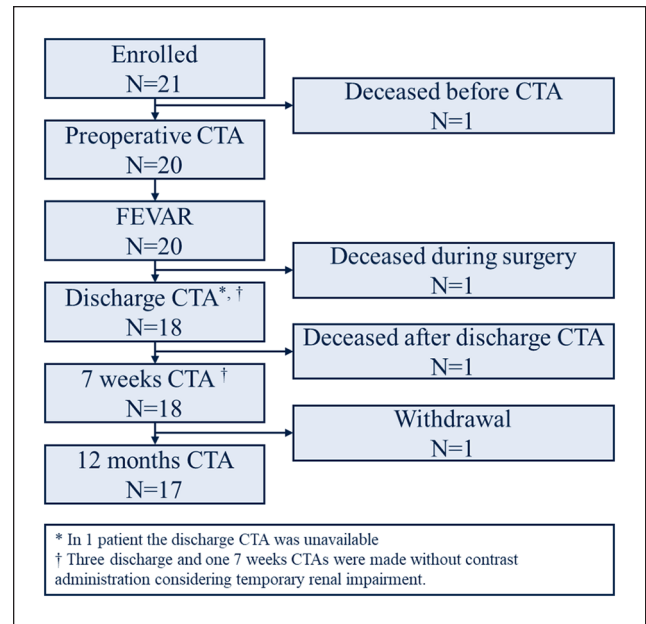


**Figure 2.** Flowchart of the patients enrolled in the LSPEAS F-EVAR trial. CTA, computed tomographic angiography, referring to electrocardiogram-gated (ECG-gated) CTA; N, number of patients.

difference  $\pm$  standard deviation (p value). Statistical significance was assumed when  $p < 0.05$ . Statistical analysis was performed using IBM SPSS statistics 28 (IBM corporation, Armonk, NY, USA).

### Results

Twenty-one patients were enrolled (Figure 2), of which one deceased of unknown cause before the preoperative CTA was made and one deceased during surgery due to major hemorrhage from a ruptured common iliac artery (CIA), resulting in 19 patients available for further analysis. After the discharge CTA, another patient passed away from cardiac decompensation. One patient withdrew before the 12-month CTA scan was performed, due to the development of Alzheimer's disease. In 1 patient, the discharge CTA was unavailable. Three discharge and one 7-week scans were made without contrast considering temporary renal impairment, according to the study protocol. Seven patients (37%) had a previous EVAR. The patient and AAA characteristics of the 19 patients eligible for analysis are shown in Table 2.

Overall, 18 right renal arteries (RRAs), 19 left renal arteries (LRAs), 15 superior mesenteric arteries (SMAs) and 8 celiac axes (CAs) were stented, all with Advanta V12 covered balloon-expandable bridging stents (Getinge, Merrimack, NH, USA). All FEVAR procedures were performed with assisted technical success rate of 95%.

**Table 2.** Patient and Aneurysm Characteristics.

Demographics	N=19 (100%)
Age—years	78 (71–80)
Male sex	19 (100%)
<b>Cardiovascular risk factors</b>	
Cigarette smoking history	16 (84%)
Hypertension	11 (58%)
Hypercholesterolemia	15 (79%)
Diabetes mellitus type	3 (16%)
Peripheral artery disease	4 (21%)
CVA and/or TIA	2 (11%)
Cardiac disease	9 (47%)
COPD gold—I/II/III	1/2/1 (21%)
Chronic kidney disease <sup>a</sup>	8 (42%)
<b>Preoperative evaluation</b>	
eGFR, mL/min/1.73 m <sup>2</sup>	59 (50–72)
Body mass index, kg/m <sup>2</sup>	26 (24–28)
ASA classification	
II	5 (26%)
III	13 (68%)
IV	1 (5%)
<b>Anatomic characteristics</b>	
Etiology—atherosclerotic <sup>c</sup>	19 (100%)
Anatomic location—juxtarenal/ pararenal/paravisceral/TAAA type IV <sup>c</sup>	9/6/3/1
Proximal sealing zone diameter—mm	29 (27–30)
Maximum aortic diameter—mm	69 (36–76)
Maximum right CIA diameter—mm	17 (14–26)
Maximum left CIA diameter—mm	15 (14–23)
Alpha angulation—degrees	24 (20–39)
Beta angulation—degrees	24 (18–43)
<b>Target arteries</b>	
CA diameter—mm	8 (7–9)
SMA diameter—mm	7 (7–8)
RRA diameter—mm	6 (5–6)
LRA diameter—mm	5 (5–6)
Number of target vessels	
2	4
3	8 <sup>b</sup>
4	7
Previous EVAR	7 (37%)

Abbreviations: ASA, American Society of Anesthesiologists; CA, celiac axis; CIA, common iliac artery; COPD, chronic obstructive pulmonary disease; CVA, cerebrovascular accident; eGFR, estimated glomerular filtration rate; EVAR, endovascular aortic aneurysm repair; LRA, left renal artery; RRA, right renal artery; SMA, superior mesenteric artery; TIA, transient ischemic attack.

<sup>a</sup>Loss of kidney function (eGFR < 60 mL/min) according to the KDIGO 2017 Clinical Practice Guidelines

<sup>b</sup>One patient had the LRA, SMA, and CA stented; not RRA.

<sup>c</sup>As defined by Wanhainen et al.<sup>23</sup>

Continuous data were presented as median (interquartile range [IQR]) and categorical data as n (%).

No neck length was defined in this table since 7 patients had a previous EVAR, so that, no neck could be defined and another 6 patients had a pararenal or paravisceral aneurysm, so that, no neck at all. The infrarenal neck could only be measured for the remaining 5 patients, being 1, 2, 3, 5, and 7 mm.

Intraoperative procedure-related complications included the above-described death after CIA rupture and a rupture of the descending thoracic aorta, intraoperatively treated with a thoracic stent-graft. Other complications included thrombus and kinking of the RRA bridging stent at 11-month follow-up, successfully treated with ballooning and additional stent placement; type Ib endoleak at 12-month follow-up, successfully treated with an extension; type Ic SMA endoleak detected on the 7-week ECG-gated CTA, successfully treated with additional stent placement; type II endoleaks in 2 patients at 3-week and 11-month follow-ups (1 did not require immediate repair, 1 was embolized, respectively); type IIIc endoleak at 2-month follow-up, suspected from SMA for which additional stent placement, but with persistent endoleak 2 months later for which additional stent placement in the CA was performed. However, the endoleak persisted without identified cause, type III not excluded.

### Dynamic and Longitudinal Target Artery Geometry and Stability

A table describing the geometrical and stability variables of the 4 target arteries at the different time points is provided as Supplemental Material.

**Branch angles** of all target arteries combined was preoperatively 58.4° (46.9–72.5°) and increased after FEVAR to 76.1° (59.1–88.9°,  $p < 0.001$ ) at discharge, to 72.9° (62.1–88.2°,  $p < 0.001$ ) at 7 weeks, and 75.1° (63.3–98.1°,  $p < 0.001$ ) at 12-month follow-up (Figure 3). The renal arteries trend to a perpendicular orientation with respect to the aorta after FEVAR: RRA branch angle increased from 60.9° (44.2–84.9°) preoperatively to 83.1° (69.0–92.7) at 7-week follow-up ( $p = 0.001$ ) and to 94.4° (72.6–99.8) at 12 months ( $p = 0.036$ ) postoperatively; LRA branch angle increased from 63.7° (55.0–73.0°) preoperatively to 79.1° (40.0–90.3°) at discharge ( $p < 0.001$ ), 85.3° (67.4–95.9°) at 7-week follow-up and to 94.3° (68.2–105.6°) at 12-month follow-up. The SMA and CA branch angles did not show a statistically significant longitudinal change. The dynamic branch angles did not seem to show changes during follow-up for all of the target vessels arteries.

**End-stent angles** did not change statistically significantly over time with an overall median of 23.6° (15.1–36.1°). The dynamic change in end-stent angle did not seem to show changes during follow-up (Figure 3).

**Curvature** means and maximums appeared stable over time, except for the dynamic mean curvature of the LRA that decreased from preoperative to 7-week follow-up by 1.09 m<sup>-1</sup> (SE=0.35, 95% CI=0.13–2.04 m<sup>-1</sup>  $p = 0.017$ ) and from preoperative to 12 months postoperative by 1.05 m<sup>-1</sup> (SE=0.36, 95% CI=0.08–2.02 m<sup>-1</sup>  $p = 0.027$ , Figure 4). To illustrate preoperatively, the LRA curvature median was 61.4 m<sup>-1</sup> with a dynamic mean curvature of 3.0 m<sup>-1</sup> that

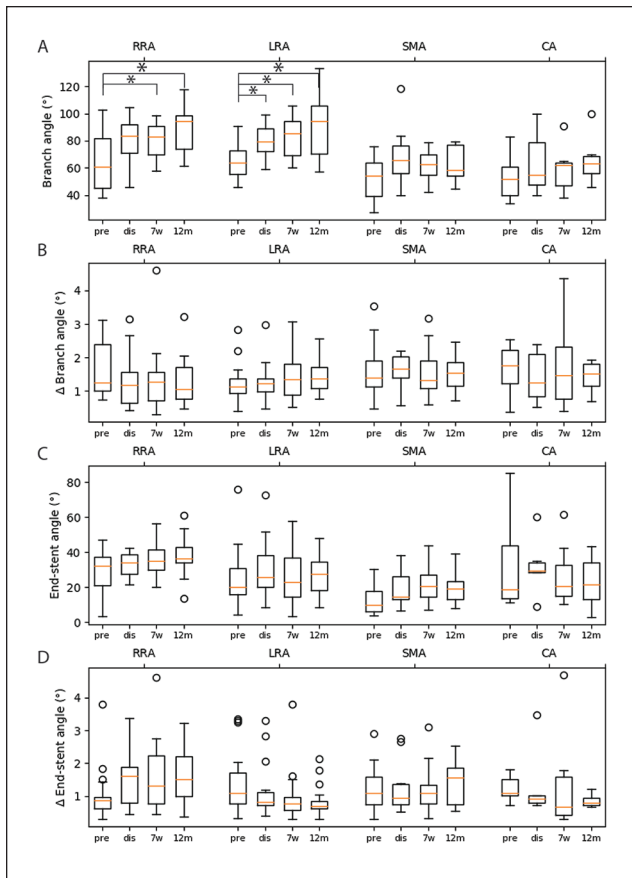


**Figure 3.** The dynamic ( $\Delta$ , A) and mid-cardiac cycle (B) branch angles and dynamic ( $\Delta$ , C) and mid-cardiac cycle (D) end-stent angles of the target arteries at the different timepoints. Pre, preoperative; dis, discharge; 7w, 7-week follow-up; 12m, 12-month follow-up; RRA, right renal artery; LRA, left renal artery; SMA, superior mesenteric artery; CA, celiac axis. \* Statistical significant difference between the 2 scan points.

corresponds to a fitted circle to the CLL with a radius ranging 15.8 to 16.7 mm (curvature  $\kappa=1/\text{radius}$  of circle). At 7-week and 12-month follow-ups, this radius ranged 21.2 to 22.2 mm. Furthermore, the location of maximal curvature and maximal dynamic curvature of the target arteries appear further downstream of the stent in the target artery after FEVAR (Figure 5). On average, the location of maximal bridging stent curvature change appears to move 4 mm downstream from discharge to 12-month follow-up, which was most pronounced for the renal arteries.

**Tortuosity index** did not seem to change during follow-up being 1.06 (1.03–1.16) preoperatively, 1.06 (1.03–1.12) at discharge, 1.07 (1.04–1.14) at 7-week follow-up, and 1.08 (1.05–1.15) at 12-month follow-up, when combined for all 4 target arteries (Figure S1 and Table S1, Supplemental Material). The dynamic TI seemed to remain stable at the different timepoints for RRA, SMA, and CA, but not for the LRA that showed a decrease of

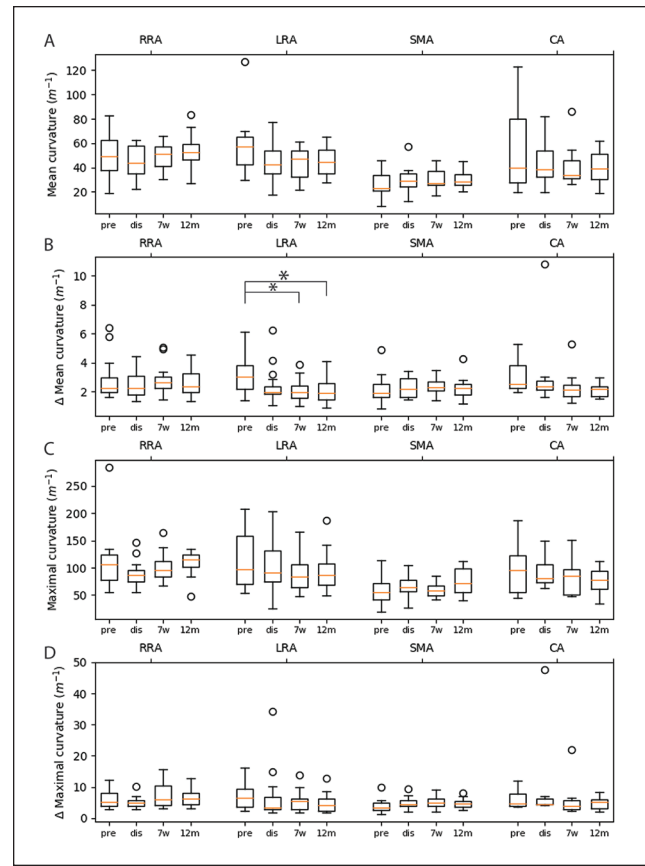


**Figure 4.** The dynamic ( $\Delta$ , A) and mid-cardiac cycle (B) mean curvature and the dynamic ( $\Delta$ , C) and mid-cardiac cycle (D) maximal curvature of the target arteries at the different timepoints. Pre, preoperative; dis, discharge; 7w, 7-week follow-up; 12m, 12-month follow-up; RRA, right renal artery; LRA, left renal artery; SMA, superior mesenteric artery; CA, celiac axis. \* Statistical significant difference between the 2 scan points.

approximately 50% of on average 0.004 (SE=0.002, 95% CI=0.000–0.009,  $p=0.030$ ).

**Body-bridging stent stability** revealed that the flare lengths were mainly below 1 cm and remained so during follow-up (Figure 6). Notably, the upstream flares were longer than the downstream flares (longer by  $1.5 \pm 2.0$  mm,  $p < 0.001$ ;  $1.5 \pm 1.3$  mm,  $p < 0.001$ ;  $1.3 \pm 1.5$  mm,  $p = 0.001$  for RRA, LRA, and CA, respectively), except for the SMA flares ( $0.2 \pm 2.1$  mm,  $p = 0.589$ ). During the cardiac cycle, the flare lengths changed  $< 0.4$  mm. The dynamic  $\text{Dist}_{\text{fen-flare-up}}$  decreased by 0.02 mm from discharge to 12-month follow-up ( $p = 0.030$ ), which could be deemed constant considering the maximal error of 0.3 mm.<sup>25</sup>  $\text{Dist}_{\text{ring-fen}}$ s were 32.1 mm (20.5–45.8) and changed up to 1.2 mm during the cardiac cycle, which did not change during follow-up. The fenestration gaps ranged up to 17 mm (SMA) and did not show statistically significant changes during follow-up. Figure 7 may suggest larger fenestration gaps for the renal

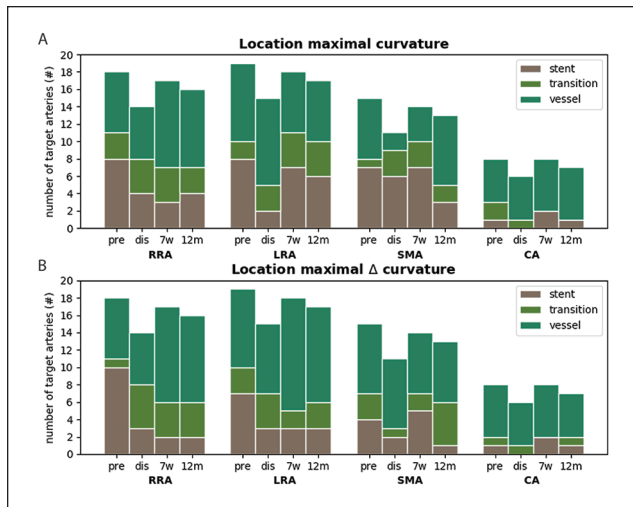


**Figure 5.** The location (stent, transition, ie, 1 cm around the end of the bridging stent, or vessel zone) of maximal dynamic ( $\Delta$ , A) and maximal mid-cardiac-cycle (B) curvature for the target arteries at the different timepoints. Note that the number of target arteries differ at the different time points due to an unavailable CTA at discharge, loss to follow-up and scans without contrast administration considering temporary renal impairment (3 discharge and one 7-week follow-up; according to protocol). RRA, right renal artery; LRA, left renal artery; SMA, superior mesenteric artery; CA, celiac axis; dis, discharge; 7w, 7-week follow-up; 12m, 12-month follow-up.

arteries than the CA, but this could not be statistically substantiated ( $p \geq 0.066$ ).

## Discussion

The present study evaluated dynamic and longitudinal geometric changes of target arteries and bridging stents up to 12 months after FEVAR with the fenestrated Anaconda with Advanta V12 bridging stents. The ECG-gated CTA assessment, using image registration and segmentation algorithms, demonstrated no significant changes in the FEVAR configurations during the cardiac cycle and over time, except for the renal branch angles increase after FEVAR toward a nearly perpendicular position to the aorta. These significantly increasing (renal) branch angles during follow-up influence the original position of the bridging stent in the target arteries and main body, which could impair sealing over time and thereby might potentially lead to endoleaks.<sup>36</sup> Conversely, the increasing renal bridging angles might also be beneficial since in non-aneurysmatic aortas, the branch angles of the renal arteries generally branch nearly perpendicular, which could also have blood flow benefits.<sup>37</sup> Remarkably, the other variables, particularly the end-stent angles, did not significantly change over the timepoints. This suggests that the increasing renal branch angles are likely to be countervailed somewhere downstream of the first bifurcation of the renal arteries.

The perpendicular adaptation of the renal bridging stent relative to the aorta after FEVAR was reported before<sup>20,38</sup> and may be attributed to the stiffness of the bridging stents that tend to straighten the native vessel. As flaring fixes the bridging stent perpendicular to the aorta in the fenestration, or with a longer upstream flare as observed in the present study, the stiffness of the bridging stents potentially promotes upward direction of the bridging stent and thereby the perpendicular orientation of the target arteries. This is probably related to the caudal placement of the bridging stents through a femoral access. Similar to our findings, Ullery et al<sup>20,38</sup> reported increasing renal branch angles by approximately  $25^\circ$ , in combination with stable end-stent angles around  $30^\circ$  and maximal curvature around  $100 \text{ m}^{-1}$  after FEVAR with Advanta V12 bridging stents, though in unspecified FEVAR stent-grafts. This supports our hypothesis that the increasing branch angle has to be compensated more downstream on the renal arteries. Ullery et al,<sup>20,38</sup> however, only investigated the renal arteries while the present study also included the analysis of 23 visceral arteries, which had steeper (smaller) branch angles compared with the renal arteries at all timepoints. This may be attributed to the naturally steeper configuration of these arteries, potentially reinforced by the compression of the diaphragm and median arcuate ligament. The orientation of the visceral bridging stents may be favorable for the patency as the native configuration is better maintained than for the renal bridging stents after FEVAR.

This is to our knowledge the first paper investigating FEVAR target vessel and bridging stent geometry for both longitudinal and cardiac-pulsatility-induced changes. Koerades et al<sup>16</sup> and Cheng et al<sup>13</sup> did investigate branch angles and end-stent angles of chimney endovascular aneurysm sealing (chEVAS) devices using ECG-gated CTA. The branch angles and end-stent angles were smaller after chEVAS, when compared with FEVAR,<sup>11,20,38</sup> which is not surprising given the position of the stents. Yet, the dynamic changes in branch angle and end-stent angle remained around  $1^\circ$  after chEVAS,<sup>13,16</sup> similar to the currently presented FEVAR results. In our present study, the dynamic branch angle and end-stent angle changes remained below  $5^\circ$ , the dynamic curvature and TI remained below, respectively,  $15 \text{ m}^{-1}$  and 0.04, which is approximately 5%, 15%, 5%, and 3% of the mid-cardiac cycle values, respectively. However, the dynamic curvature and dynamic TI of the LRAs decreased after FEVAR, suggesting stiffening of the branch artery. As can be seen in Figure 4, the decrease dynamic in curvature for the LRA originates from a relatively large preoperative mean curvature for the LRA. In the data, no clear explanation could be identified although an explanation might lie in the left kidney being located caudally from the heart and thereby may be influenced by the motion of the heart. Interestingly, Kahlberg et al<sup>39</sup> reported a lower patency rate of the LRA as compared with other abdominal aortic branches after open repair of thoracoabdominal aortic aneurysms. They suggest that



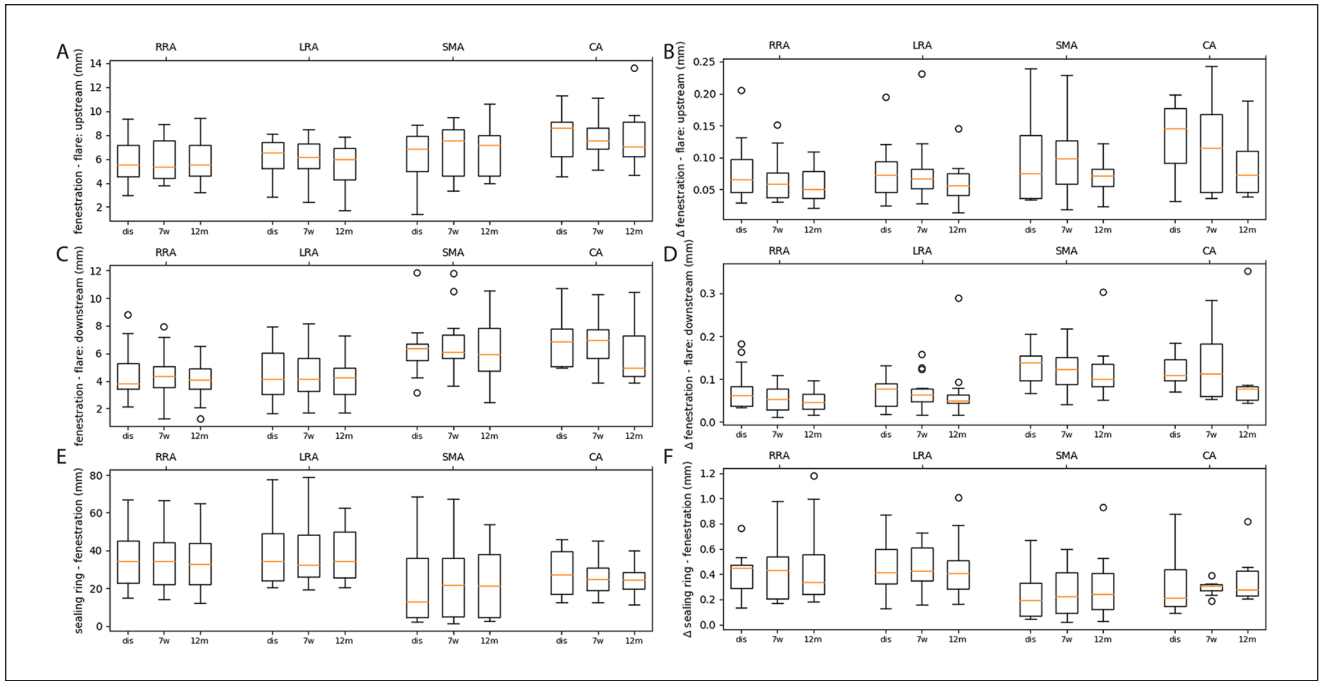


**Figure 6.** The mid-cardiac cycle (left) and dynamic ( $\Delta$ , right) upstream flare length (A and B, respectively), downstream flare length (C and D, respectively) and the distance between the proximal sealing ring and fenestration (E and F, respectively) are shown at the different postoperative timepoints. RRA, right renal artery; LRA, left renal artery; SMA, superior mesenteric artery; CA, celiac axis; dis, discharge; 7w, 7-week follow-up; 12m, 12-month follow-up. No statistically significant longitudinal changes were observed.

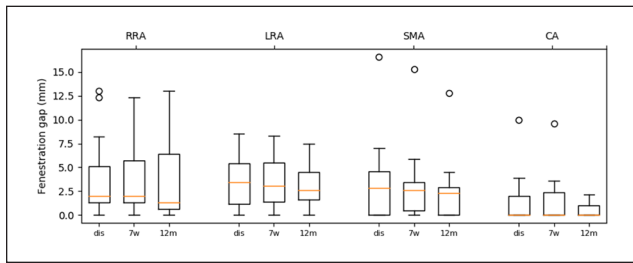


**Figure 7.** The mid-cardiac cycle fenestration gaps for the different target arteries at the postoperative timepoints. RRA, right renal artery; LRA, left renal artery; SMA, superior mesenteric artery; CA, celiac axis; dis, discharge; 7w, 7-week follow-up; 12m, 12-month follow-up. No statistically significant longitudinal changes were observed.

repositioning and subsequent angulation of the branch may play a role in the patency loss, which may suggest that the LRA is more prone to patency loss after any form of complex AAA repair. Thereby, the higher position and less fixed environment, that is, no liver that could limit the displacement, may also play a role in the difference in behavior of right and left renal bridging stents. Although the dynamic curvature and TI decreases did not lead to complications within the first-year follow-up, it is important to consider the potential future consequences of this low conformability. The bridging stent flare lengths were constant as these did not change more than

the empirically defined error ( $<0.3$  mm)<sup>15</sup>. The dynamic stent-ring fenestration distances ranged up to 1.2 mm, which can probably be attributed to the larger pulsatile motion of the suprarenal aorta in which the proximal stent-ring is situated.<sup>12</sup>

Despite the current observations on the stability and the encouraging clinical results<sup>2,7-10</sup> of the stent-graft no robust conclusions can be drawn at this stage, solely on these data. It is important to emphasize that the respiratory cycle could also be of influence on the durability of FEVAR as the visceral arteries are close to the diaphragm and the kidney's positions are influenced by breathing.<sup>40,41</sup> For example, Ullery et al<sup>11</sup> found respiratory-induced change in branch angles and end-stent angles of approximately  $5^\circ$  in stented renal arteries in 11 FEVAR patients. The limited cardiac-pulsatility-induced and respiratory-induced geometry changes may be favorable in terms of material fatigue of the bridging stents and minimal blood flow disturbances, reducing the risk of thrombus formation.

Three patients in the present study presented with bridging stent-related complications. The type Ic endoleak of one patient's SMA was due to a too short bridging stent ending in the aneurysm lumen/dilated origin of SMA, this may not be considered graft failure, but rather insufficient stent sizing and/or positioning. This was also reflected in the large fenestration gap that decreased during follow-up (discharge: 17 mm, 7 weeks: 15 mm, 12 months: 13 mm). The SMA

with a type IIIc endoleak at 2-month follow-up had an above average increase in the SMA branch angle and dynamic branch angle change from preoperative to postoperative ( $31^{\circ}$ – $56^{\circ}$  and  $2.1^{\circ}$ – $2.7^{\circ}$ , respectively), while the end-stent angle decreased  $15^{\circ}$ . The dynamic SMA end-stent angle decreased after relining of the SMA ( $0.3^{\circ}$ ). Thereby, the fenestration gap of the RRA was large (ca. 12 mm), but it is unclear if this may have played a role in the persisting endoleak. The RRA with bridging stent thrombosis and kinking demonstrated a relatively large increase in end-stent angle from preoperative ( $10^{\circ}$ ) to discharge ( $33^{\circ}$ ) and to 7 weeks ( $42^{\circ}$ ), as well as in dynamic end-stent angle change with  $1.1^{\circ}$ ,  $1.7^{\circ}$ , and  $2.5^{\circ}$ , respectively. However, (dynamic) end-stent angle and fenestration gap were not significantly affected by the relining (end-stent angle to  $38^{\circ}$ , dynamic end-stent angle to  $2.2^{\circ}$  and fenestration gap to 1 mm at 12-month follow-up, the endpoint of the study). Although these results should be interpreted with care, significant geometry alterations, such as a large increase in (dynamic) branch angle, a decrease in end-stent angle and significant postoperative changes in distances between device components may increase the risk for endoleaks. Likewise, large (dynamic) end-stent angles may increase the risk for kinking, stenosis, or occlusion. These results emphasize the importance of avoiding major geometrical deformation during stent-graft placement, and of conformability of stent-grafts to the aorta and bridging stents to the target arteries. This may be achieved by choosing more conformable types of bridging stents.

### Limitations

End-stent angles and the maximal curvature locations could not be calculated in all CTAs, as some of these scans were made without contrast agent administration in patients with postoperative renal function impairment, according to protocol. Furthermore, the relatively small sample size of the study in combination with the heterogeneity of the aneurysm types may be considered a limitation as well. These factors potentially limit the generalizability of the outcomes and could induce statistical type II errors. However, this study was not designed to evaluate the relation between clinical outcomes and stent-graft deformation, but rather to evaluate in detail the dynamic and longitudinal behavior of the stented target arteries and bridging stents to improve our understanding about the device durability under cardiac loading that may prove essential in future treatment improvement. Still, significant dynamic and longitudinal deformation was observed and potential clinical implications were identified. Moreover, routine performance of ECG-gated CT would provide additional insights in factors potentially influencing treatment durability in an earlier stage and in fewer patients than achievable with large

registries. Therefore, it is key to spread the knowledge regarding the analysis of ECG-gated CT scans through papers like this.

### Conclusion

This prospective study provided detailed insights into the dynamic geometric behavior of the fenestrated Anaconda with Advanta V12 bridging stents up to 12-month follow-up. The end-stent angles, curvature, TI, and fenestration gap of the target arteries appeared to remain stable during FEVAR and throughout the follow-up period. Interestingly, the renal branch angles increase toward a perpendicular orientation with respect to the aorta following FEVAR. In future research, the aim will be to investigate all dynamic aspects, also including the respiratory cycle and blood flow, of FEVAR with a variety of stent-graft combinations to optimize treatment for all aneurysm patients.

### Acknowledgments

The authors are grateful for the support of the full LSPEAS F-EVAR consortium and all CT technicians that made this study possible.

### Declaration of Conflicting Interests

The author(s) declared the following potential conflicts of interest with respect to the research, authorship, and/or publication of this article: This work was funded by unrestricted grants from Terumo Aortic and by the PPP Allowance made available by Health-Holland, Top Sector Life Sciences & Health. Permission to publish the results was not needed. Prof. Dr R.H. Geelkerken, Prof. Dr M.M.P.J. Reijnen and Prof. Dr C.J.A.M. Zeebregts are consultants for Terumo Aortic.




### Funding

The author(s) disclosed receipt of the following financial support for the research, authorship, and/or publication of this article: This work was funded by unrestricted grants from Terumo Aortic and by the PPP Allowance made available by Health-Holland, Top Sector Life Sciences & Health. Permission to publish the results was not needed.

### Prior Presentation

Part of the work described in this manuscript was presented during the defense of the dissertation of the first author (J.A. Simmering, Endovascular Repair of the Aorta: Stent-graft deformation matters, April 14, 2023, Enschede, The Netherlands) and during the 36th ESVS conference (September 20, 2023, Rome, Italy).

### ORCID iDs

Jaimey A. Simmering  <https://orcid.org/0000-0002-6178-1635>  
Maaikje A. Koenrades  <https://orcid.org/0000-0003-4555-0551>  
Erik Groot Jebbink  <https://orcid.org/0000-0001-7041-8603>

## Supplemental Material

Supplemental material for this article is available online.

## References

- Huang IKH, Renani SA, Morgan RA. Complications and reinterventions after fenestrated and branched evar in patients with paravisceral and thoracoabdominal aneurysms. *Cardiovasc Intervent Radiol*. 2018;41(7):985–997. doi:10.1007/s00270-018-1917-0.
- Dijkstra ML, Tielliu IFJ, Meerwaldt R. Dutch experience with the fenestrated Anaconda endograft for short-neck infrarenal and juxtarenal abdominal aortic aneurysm repair. *J Vasc Surg*. 2013;60(2):301–307. doi:10.1016/j.jvs.2014.02.011.
- Rolls AE, Jenkins M, Bicknell CD, et al. Experience with a novel custom-made fenestrated stent graft in the repair of juxtarenal and type IV thoracoabdominal aneurysms. *J Vasc Surg*. 2014;59(3):615–622. doi:10.1016/j.jvs.2013.10.038.
- Gallitto E, Faggioli G, Melissano G, et al. Preoperative and postoperative predictors of clinical outcome of fenestrated and branched endovascular repair for complex abdominal and thoracoabdominal aortic aneurysms in an Italian multicenter registry. *J Vasc Surg*. 2021;74(6):1795–1806. doi:10.1016/j.jvs.2021.04.072.
- Midy D, Becquemin J, Mialhe C, et al. Results of the French multicentric study of anaconda fenestrated endografts in the treatment of complex aortic pathologies (EFEFA Registry). *Ann Vasc Surg*. 2017;43:151–165. doi:10.1016/j.avsg.2017.03.171.
- Zlatanovic P, Mascia D, Ancetti S, et al. Short term and long term clinical outcomes of endovascular versus open repair for juxtarenal and pararenal abdominal aortic aneurysms using propensity score matching: results from Juxta- and pararenal aortic Aneurysm Multicentre European Study (JAMES). *Eur J Vasc Endovasc Surg*. 2023;65(6):828–836. doi:10.1016/j.ejvs.2023.02.070.
- Falkensammer J, Taher F, Uhlmann M, et al. Rescue of failed endovascular aortic aneurysm repair using the fenestrated Anaconda device. *J Vasc Surg*. 2017;66(5):1334–1339. doi:10.1016/j.jvs.2017.02.048.
- Blankensteijn LL, Dijkstra ML, Tielliu IFJ, et al. Midterm results of the fenestrated Anaconda endograft for short-neck infrarenal and juxtarenal abdominal aortic aneurysm repair. *J Vasc Surg*. 2017;65(2):303–310. doi:10.1016/j.jvs.2016.08.092.
- Roy IN, Millen AM, Jones SM, et al. Long-term follow-up of fenestrated endovascular repair for juxtarenal aortic aneurysm. *Br J Surg*. 2017;104(8):1020–1027. doi:10.1002/bjs.10524.
- Tinelli G, Bonnet M, Hertault A, et al. Impact of hybrid operating rooms on long-term clinical outcomes following fenestrated and branched endovascular aortic repair. *J Endovasc Ther*. 2021;28(3):415–424. doi:10.1177/1526602821996725.
- Ullery BW, Suh GY, Lee JT, et al. Geometry and respiratory-induced deformation of abdominal branch vessels and stents after complex endovascular aneurysm repair. *J Vasc Surg*. 2015;61(4):875–884. doi:10.1016/j.jvs.2014.11.075.
- Muhs BE, Teutelink A, Prokop M, et al. Endovascular aneurysm repair alters renal artery movement: a preliminary evaluation using dynamic CTA. *J Endovasc Ther*. 2006;13(4):476–480.
- Cheng CP, Suh GY, Kim JJ, et al. Cardiac pulsatility- and respiratory-induced deformations of the renal arteries and snorkel stents after snorkel endovascular aneurysm sealing. *J Endovasc Ther*. 2019;26(4):556–564. doi:10.1177/1526602819856363.
- Koenrades MA, Klein A, Lefterink AM, et al. Evolution of the proximal sealing rings of the anaconda stent-graft after endovascular aneurysm repair. *J Endovasc Ther*. 2018;25(4):480–491. doi:10.1177/1526602818773085.
- Koenrades MA, Struijs EM, Klein A, et al. Quantitative stent-graft motion in ECG-gated CT by image registration and segmentation: in vitro validation and preliminary clinical results. *Eur J Vasc Endovasc Surg*. 2019;58(5):746–755. doi:10.1016/j.ejvs.2019.03.009.
- Koenrades MA, Donselaar EJ, van Erp MAJM, et al. Electrocardiography-gated computed tomography angiography analysis of cardiac pulsatility-induced motion and deformation after endovascular aneurysm sealing with chimney grafts. *J Vasc Surg*. 2020;72(5):1743–1752. doi:10.1016/j.jvs.2020.01.064.
- Simmering JA, Slump CH, Geelkerken RH, et al. Geometrical change in Anaconda endograft limbs after endovascular aneurysm repair: a potential predictor for limb occlusion. *Semin Vasc Surg*. 2019;32(3–4):94–105. doi:10.1053/j.semvasc-surg.2019.11.001.
- van Helvert M, Simmering JA, Koenrades MA, et al. Evaluation of ECG-gated CTA to quantify changes in geometry and dynamic behavior of the iliac artery after placement of the Gore Excluder Iliac Branch Endoprosthesis. *J Cardiovasc Surg (Torino)*. 2022;63:454–463. doi:10.23736/S0021-9509.22.11980-4.
- Koenrades MA, Bosscher MRF, Ubink JT, et al. Geometric remodeling of the perirenal aortic neck at and adjacent to the double sealing ring of the anaconda stent-graft after endovascular aneurysm repair. *J Endovasc Ther*. 2019;26(6):855–864. doi:10.1177/1526602819882379.
- Ullery BW, Suh G-Y, Lee JT, et al. Comparative geometric analysis of renal artery anatomy before and after fenestrated or snorkel/chimney endovascular aneurysm repair. *J Vasc Surg*. 2016;63(4):922–929. doi:10.1016/j.jvs.2015.10.091.
- Muhs BE, Vincken KL, van Prehn J, et al. Dynamic cine-CT angiography for the evaluation of the thoracic aorta; insight in dynamic changes with implications for thoracic endograft treatment. *Eur J Vasc Endovasc Surg*. 2006;32(5):532–536. doi:10.1016/j.ejvs.2006.05.009.
- Draney MT, Zarins CK, Taylor CA. Three-dimensional analysis of renal artery bending motion during respiration. *J Endovasc Ther*. 2005;12(3):380–386. doi:10.1583/05-1530.1.
- Wanhainen A, Verzini F, Van Herzelee I, et al. European Society for Vascular Surgery (ESVS) 2019 clinical practice guidelines on the management of abdominal Aorto-iliac artery aneurysms. *Eur J Vasc Endovasc Surg*. 2019;57(1):8–93. doi:10.1016/j.ejvs.2018.09.020.
- Oderich GS, Forbes TL, Chaer R, et al. Reporting standards for endovascular aortic repair of aneurysms involving the renal-mesenteric arteries. *J Vasc Surg*. 2020;73(1):4S–52S. doi:10.1016/j.jvs.2020.06.011.
- Koenrades MA, Struijs EM, Klein A, et al. Validation of an image registration and segmentation method to measure stent

- graft motion on ECG-gated CT using a physical dynamic stent graft model. *Med Imaging 2017 Comput Diagnosis*. 2017;10134:1013418. doi:10.1117/12.2254262.
26. Klein A, Kroon D-J, Hoogeveen Y, et al. Multimodal image registration by edge attraction and regularization using a B-spline grid. *Med Imaging 2011 Image Process*. 2011;7962:796220. doi:10.1117/12.878267.
  27. Klein A, Renema WKJ, van der Vliet JA, et al. Motion calculations on stent grafts in AAA. In: Grundmann RT, ed. *Diagnosis, Screening and Treatment of Abdominal, Thoracoabdominal and Thoracic Aortic Aneurysms*. Rijeka, Croatia: Intechopen; 2011:125–144.
  28. Klein A, van der Vliet JA, Oostveen LJ, et al. Automatic segmentation of the wire frame of stent grafts from CT data. *Med Image Anal*. 2012;16(1):127–139. doi:10.1016/j.media.2011.05.015.
  29. Simmering JA, de Vries M, Haalboom M, et al. Geometrical changes of the aorta as predictors for thromboembolic events after EVAR with the anaconda stent-graft. *J Endovasc Ther*. 2022;2:1526660282211058. doi:10.1177/152666028221105839.
  30. Simmering JA, Leeuwerke SJG, Meerwaldt R, et al. In vivo quantification of cardiac-pulsatility-induced motion before and after double-branched endovascular aortic arch repair. *J Endovasc Ther*. 2023;30:510–519. doi:10.1177/152666028221086474.
  31. Schuurmann RCL, Ouriel K, Muhs BE, et al. Aortic curvature as a predictor of intraoperative type Ia endoleak. *J Vasc Surg*. 2016;63(3):596–602. doi:10.1016/j.jvs.2015.08.110.
  32. Schuurmann RCL, Van Noort K, Overeem SP, et al. Aortic curvature is a predictor of late type Ia endoleak and migration after endovascular aneurysm repair. *J Endovasc Ther*. 2017;24(3):411–417. doi:10.1177/15266602817700378.
  33. Schuurmann RCL, Kuster L, Slump CH, et al. Aortic curvature instead of angulation allows improved estimation of the true aorto-iliac trajectory. *Eur J Vasc Endovasc Surg*. 2016;51(2):216–224. doi:10.1016/j.ejvs.2015.09.008.
  34. Lorensen WE, Cline HE. Marching Cubes: a high resolution 3D surface construction algorithm. *Comput Graph (ACM)*. 1987;21(4):163–169.
  35. Chait J, Tenorio ER, Mendes BC, et al. Impact of gap distance between fenestration and aortic wall on target artery instability following fenestrated-branched endovascular aortic repair. *J Vasc Surg*. 2022;76(1):79–87. doi:10.1016/j.jvs.2022.01.135.
  36. Ou J, Tang AYS, Chiu TL, et al. Haemodynamic variations of flow to renal arteries in custom-made and pivot branch fenestrated endografting. *Eur J Vasc Endovasc Surg*. 2017;53(1):133–139. doi:10.1016/j.ejvs.2016.10.022.
  37. Tucker T. Physics linkages between arterial morphology, pulse wave reflection and peripheral flow. *Artery Res*. 2023;29(2):46–71. doi:10.1007/s44200-023-00033-5.
  38. Ullery BW, Suh G, Kim JJ, et al. Dynamic geometric analysis of the renal arteries and aorta following complex endovascular aneurysm repair. *Ann Vasc Surg*. 2017;43:85–95. doi:10.1016/j.avsg.2016.12.005.
  39. Kahlberg A, Ferrante AMR, Miloro R, et al. Late patency of reconstructed visceral arteries after open repair of thoracoabdominal aortic aneurysm. *J Vasc Surg*. 2018;67(4):1017–1024. doi:10.1016/j.jvs.2017.08.067.
  40. Muhs BE, Vincken KL, Teutelink A, et al. Dynamic cine-computed tomography angiography imaging of standard and fenestrated endografts: differing effects on renal artery motion. *Vasc Endovascular Surg*. 2008;42(1):25–31. doi:10.1177/1538574407308200.
  41. Suh G-Y, Choi G, Herfkens RJ, et al. Three-dimensional modeling analysis of visceral arteries and kidneys during respiration. *Ann Vasc Surg*. 2016;34:250–260. doi:10.1016/j.avsg.2016.04.004.